Nat. Hazards Earth Syst. Sci. Discuss., doi:10.5194/nhess-2016-167, 2016
Manuscript under review for journal Nat. Hazards Earth Syst. Sci.
Published: 31 May 2016

Natural Hazards and Earth System Sciences
Open Access
Discussions

Development of fragility curves for railway ballast and embankment scour due to overtopping flood flow

Ryota Tsubaki[1*], Koji Ichii[2], Jeremy D Bricker[3] and Yoshihisa Kawahara[2]

[1] Department of Civil Engineering, Nagoya University, Nagoya, Aichi, Japan

[2] Department of Civil and Environmental Engineering, Hiroshima University, Higashi-hiroshima, Hiroshima, Japan

[3] International Research Institute of Disaster Science, Tohoku University, Sendai, Miyagi, Japan

[*] E-mail: rtsubaki@civil.nagoya-u.ac.jp

Abstract

Fragility curves evaluating risk of railway track ballast and embankment fill scour were developed. To develop fragility curves, two well-documented single-track railway washouts during two recent floods in Japan were investigated. Type of damage to the railway was categorized into no damage, ballast scour, and embankment scour, in order of damage severity. Railway overtopping surcharge for each event was estimated via hydrologic and hydraulic analysis. Normal and log-normal fragility curves were developed based on failure probability derived from field records. A combined ballast and embankment scour model was validated by comparing the spatial distribution of railway scour with the field damage record.

Key Words: railway embankment, fragility curve, overtopping, ballast scour, embankment scour

1. Introduction

Railway lines consist of components including tracks, power supply, and signaling infrastructure, all of which can suffer damage during river floods, hurricane storm surge, and tsunamis, leading to interruption of transportation service (see Figure 1 for two examples for damage due to surge in the USA). The most common mechanism of track damage occurs when tracks are overtopped by floodwaters, leading to scouring of the ballast and/or the embankment fill upon which the rail tracks are built. Even when only a short section of track is washed out, the entire railway system can experience serious delays or malfunction due to a ripple effect on the dispatch of engines and cars until the damaged section is repaired.

Since railcars (except those specialized for steep slopes like cable cars or rack railways) cannot handle steep gradients in topography, railways are often built in areas of mild slopes, such as rivers, floodplains, and coasts. Due to this, railway damage is a common occurrence during flood events (e.g. Changnon 2009, Polemio et al. 2011, Tsubaki et al. 2012b). Furthermore, railways utilize many bridges, which are often built with low clearance over waterways in order to minimize construction time, cost, and track slope. Many examples exist of such bridges collapsing during large river flood and tsunami events (e.g. Wardhana and Hadipriono 2003, Reed et al. 2004, Kaneko 2010).

As such, railways are seen to exhibit significant vulnerability when tracks are inundated or overtopped. Climate change projections show that in some locations, the frequency and intensity of river flood and storm surge events will increase (IPCC 2014), further exacerbating risk to railway damage due to overtopping and inundation. Predictive evaluation of railway damage due to flood is essential for concrete assessment of socio-economic impact of large flood events.

HAZUS is a software package for estimating potential losses caused by earthquakes, floods and hurricanes used in the USA. Within the framework of HAZUS, a railway system consists of railway track/embankments, bridges, tunnels, stations, and other facilities (FEMA 2010a, 2010b, 2010c, see Table 1 for the items accounted in the flood sub-model in HAZUS). In HAZUS, damage to railway tracks due to earthquakes is evaluated based on permanent ground deformation (p.7-25, FEMA 2010a), and the damage functions developed for major roads are adopted for damage estimation for railway tracks/roadbeds (p.7-32, FEMA2010a). However, there is no guideline to estimate damage to railway tracks due to floods or hurricanes in the HAZUS framework. There have been several attempts to establish failure prediction of railway components (e.g. Argyroudis and Kaynia 2014) and river embankments (e.g. Hata et al. 2015) for damage due to seismic motion; however railway track/embankment fragility due to flood overtopping is not yet implemented in practice (FEMA 2010b). Fundamental research on the processes responsible for railway embankment failure during floods has recently begun. For example, Polemio and Lollino 2011 reported a case of seepage failure of railway embankment. Tsubaki et al. 2012a experimentally investigated the process and critical condition of ballast breaching.

In Japan, rapid population decline is another factor exacerbating risk to railways in many regions, as the amount of money available for maintenance and upgrade of these railroads is shrinking together with the amount of customers and goods they serve to transport. Therefore, in order to prevent the need for expensive repairs after damage during future events, it is essential to evaluate which sections of railroads are most vulnerable to washout during floods and to strengthen these sections before damage occurs.

Nat. Hazards Earth Syst. Sci. Discuss., doi:10.5194/nhess-2016-167, 2016
Manuscript under review for journal Nat. Hazards Earth Syst. Sci.
Published: 31 May 2016

Natural Hazards and Earth System Sciences
Discussions

Table 1 Railway System Classifications in HAZUS (2010b)

Occupancy	HAZUS valuation in thousands of dollars
Railway Tracks (per km)	1,500
Railway Bridge (Concrete, steel, wood and unknown types)	5,000
Railway Tunnel	10,000
Railway Urban Station (Concrete, steel, wood and brick made)	2,000
Railway Fuel Facility (Tanks)	3,000
Railway Dispatch Facility (Equip)	3,000
Railway Maintenance Facility (Concrete, steel, wood and brick made)	2,800

This paper focuses on fragility estimation of railway track/embankment scour due to overtopping. Even though railway embankments are geometrically similar to roadway embankments and levees, the structures atop railway embankments are very different from those atop these other embankments, as are the mechanisms by which overtopping can cause damage. As Figure 2 shows, floods can cause damage to railroad embankments via three processes: (a) scour of ballast induced by overtopping, (b) scour of both ballast and embankment fill by overtopping, and (c) piping/seepage failure of embankment fill. Though piping/seepage failure of fill is more likely to occur in high embankments, most railway embankments are relatively low, and most observed railway embankment failures appear to have been the result of overtopping-induced scour of fill and/or ballast (Kaneko 2010, Tsubaki et al. 2012b, Onoda et al. 2015). In the cases of ballast scour only, repair of the ballast layer is relatively straightforward, but in cases of embankment fill scour, repairs can be costly and take a long time. Repair of damage to an embankment is less expensive than repair of damage to bridges and other facilities (see Table 1), but ballast and embankment damage occurs much more frequently than bridge damage. Furthermore, river floods or tsunamis large enough to damage bridges usually also cause severe flooding which leads very long sections of embankment to wash out (e.g. Shimozono and Sato 2016). Therefore, the development of fragility curves for scour of railroad ballast and embankments is crucial for assessment of railroad vulnerability and resilience.

Fragility curves are widely used to evaluate the vulnerability of structures in terms of probability (Shinozuka et al. 2000). This approach was initially applied for seismic damage to bridges and other structures (Shinozuka et al. 2000, Ichii 2002, Hata el al. 2015), and application to water related hazards has followed (e.g. Hall et al. 2003 for national-scale flood risk assessment, Vorogushyn et al. 2009 for embankment piping

Nat. Hazards Earth Syst. Sci. Discuss., doi:10.5194/nhess-2016-167, 2016
Manuscript under review for journal Nat. Hazards Earth Syst. Sci.
Published: 31 May 2016

failure, Suppasri et al. 2012 for building damage due to tsunami).

The manner in which earthquakes damage earthen embankments is relatively simple and understood, even though the exact physical/dynamic properties of earth fill, especially the spatial distribution, are usually uncertain. Floods, on the other hand, interact with and are controlled by the presence of embankments. There are even many locations in which transportation embankments serve as de facto river and coastal levees (e.g. Brammer 1990, Ueda and Nakatsuka 2014). In such a location, if a flood causes an embankment breach, the flood will spread to previously protected areas. Therefore, in evaluating the risk of damage due to a railway embankment breach, it's important to evaluate the effect of that breach on the spread of the flood itself. Predicting the location of the railway embankment having significant potential to scour is essential to precisely evaluate the effect of the embankment breaching on the flood propagation during catastrophic flood events.

This paper investigates the conditions responsible for washout of track ballast and embankment fill for single-track, unelectrified railroads, which are quite common in rural areas where the level of flood protection is relatively limited. The fragility curves for this kind of railway embankment are developed based on two well-documented rail track washout events during the recent floods in Japan. To develop fragility curves, damage from each of these events is compared with embankment overtopping surcharge, which is estimated via hydrologic and hydraulic analysis. The spatial distribution of railway embankment scour evaluated using developed fragility curves is then compared with damage recorded in the field. Finally, the validity, limitations, and required further research regarding the development of fragility curves for railway embankment scour are discussed.

Figure 1 Railway embankment scour failures (left: New Jersey Transit tracks in New Jersey, USA after Hurricane Sandy in 2012; right: CSX railroad tracks in Mississippi, USA after Hurricane Katrina in 2005)

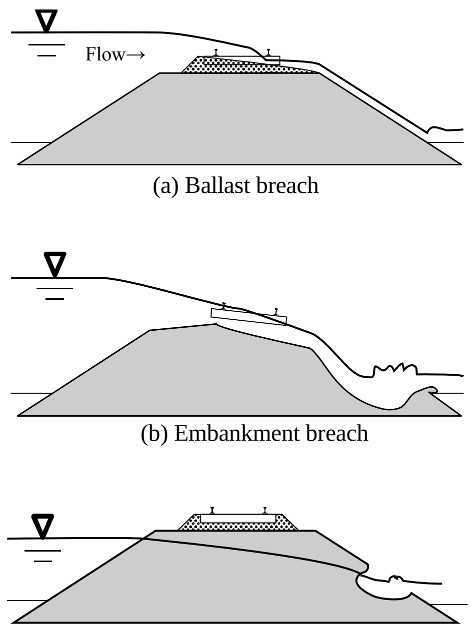

Figure 2 Railway embankment failure types.

2. Target events

2.1 Asa River flood of July, 2010

In June 2010, a large flood occurred in the Asa River including section M in the basin, causing inundation of homes and a factory, as well as washout of a railroad embankment (Tsubaki et al. 2014). The left-hand map in Figure 3 outlines the watershed upstream of section M of the Asa River in red, while the watershed of the entire reach of the Asa River is outlined in orange. A hydrologic model calculated the maximum flow rate in the Asa River to be 811 m^3/s (personal communication with Yamaguchi Prefecture), while the inflow from the Zuiko River was 110 m^3/s. Though it's possible that the peak flow in each river would reach their confluence at slightly different times, the same hydrologic model showed that the maximum flow at a point 3 km downstream of the confluence was 967 m^3/s. This flow rate closely matches that calculated from high water marks measured in the field. Since no major tributaries exist between the confluence of the two rivers and this measurement point, flow rates of 811 m^3/s for the Asa River and 110 m^3/s for the Zuiko River are adopted as steady inflow boundary conditions of the hydraulic model of section M.

Nat. Hazards Earth Syst. Sci. Discuss., doi:10.5194/nhess-2016-167, 2016
Manuscript under review for journal Nat. Hazards Earth Syst. Sci.
Published: 31 May 2016

Natural Hazards and Earth System Sciences
Open Access
Discussions

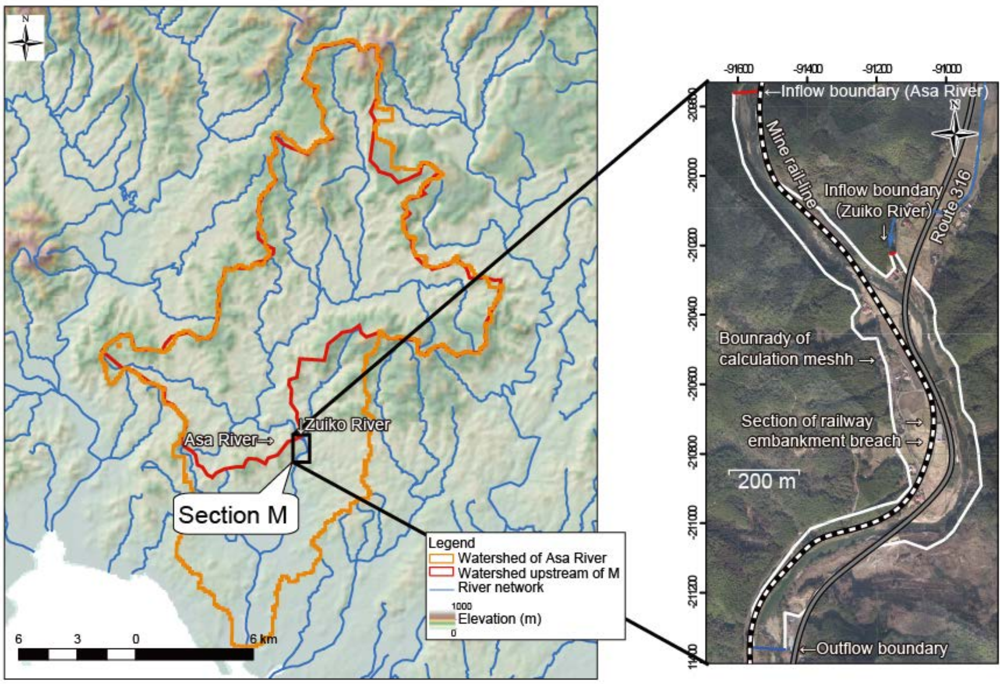

Figure 3 Watershed of the Asa River (left) and aerial photo of section M (right).

2.2 Sayo River flood of August, 2009

On August 8-11, 2009, Typhoon Etau generated record rainfall over the mid-west region of Japan including Sayo Town, Hyogo Prefecture. The previous 24-hour record rainfall in Sayo Town had been 187 mm, but Typhoon Etau set a new record at 327 mm. This caused record flooding in the Chigusa River, the watershed of which includes Sayo Town and much of western Hyogo Prefecture, resulting in a large number of casualties, as well as extensive damage to river and slope protection works (Tsubaki et al. 2012b).

Figure 4 (left panel) illustrates the watershed upstream of section S of the Sayo River, together with that of its primary river, the Chigusa River. Figure 4 (right panel) depicts the domain in which the hydraulic flood model was evaluated. The highest flow rate that passed through here during the August 2009 storm was calculated to be 750 m^3/s by hydrologic and hydraulic analysis conducted in Fujita et al. 2012.

Nat. Hazards Earth Syst. Sci. Discuss., doi:10.5194/nhess-2016-167, 2016
Manuscript under review for journal Nat. Hazards Earth Syst. Sci.
Published: 31 May 2016

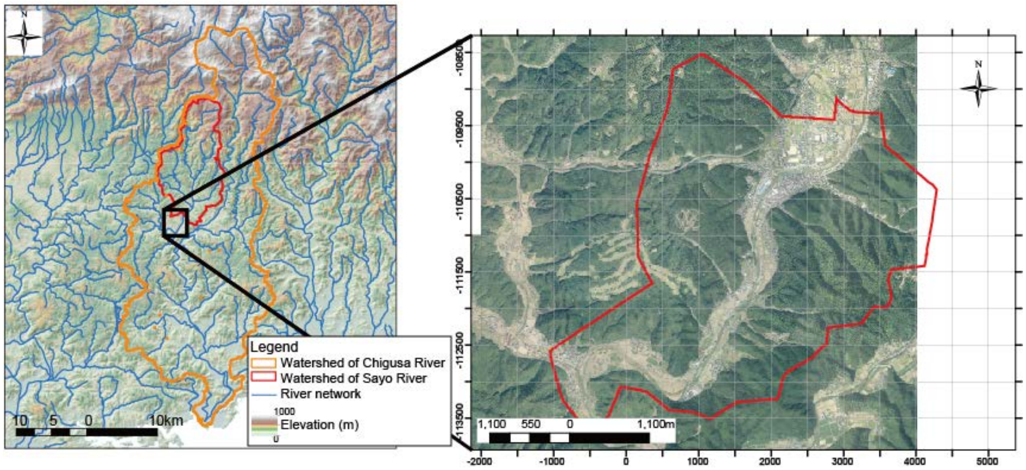

Figure 4 Watershed of Sayo River section S (left) and hydraulic flood model domain (right).

3. Methods

3.1 Fragility curve

In this paper, we use upstream flood water level (surcharge) as an explanatory variable for railway breaching failures. Under the situation of water overtopping an embankment, critical flow occurs on the embankment and the upstream water level correlates almost directly to the overtopping discharge. The upstream water has less velocity head and the surface is relatively flat, whereas the overtopping flow atop the embankment is rapidly-varied flow and quite sensitive to small differences and uncertainty in the local elevation of the embankment crest. The local flow rate over complex topography (i.e., an embankment crest) estimated by an inundation simulation has non-negligible uncertainty even though a fine calculation grid (one to few meters spacing) was used, but the estimated upstream water level has a smaller relative uncertainty (Tsubaki and Kawahara 2013). For these reasons we use the upstream water level to explain the probability of embankment failure.

Properties of ballast, embankment fill and surface cover of the embankment vary depending on the region/country/design standard of the railway being investigated, as well as on the characteristics of the specific cross sections of interest. The two railway lines focused on in this paper are single-track, unelectrified railroads running through mountainous regions, and which started operation about 90 years ago. In this regard, the material properties of the railways are relatively homogeneous.

In the fragility curve approach, a probabilistic damage function can be expressed by a two parameter normal

Nat. Hazards Earth Syst. Sci. Discuss., doi:10.5194/nhess-2016-167, 2016
Manuscript under review for journal Nat. Hazards Earth Syst. Sci.
Published: 31 May 2016

distribution function (Shinozuka et al. 2000, Suppasri et al. 2012),

$$F(a) = \Phi\left[{a - \mu}/{\sigma} \right] \tag{1}$$

or log-normal distribution function

$$F(a) = \Phi\left[{\ln(a/c)}/{\zeta} \right] \tag{2}$$

where $F(\ )$ represents the conditional probability of occurrence for the specific state of damage; Φ is the normal error function; a represents the hazard level; μ and σ are the median and standard deviation of hazard level; and c and ζ are the median and log-standard deviation, respectively. The deviation parameters σ or ζ represent both uncertainty in hazard level a and variation in fragility among data points. The estimation of the two model parameters (median and deviation) is carried out by maximizing the likelihood function. The likelihood function for binary damage (damage / no damage) is

$$L = \prod_{i=1}^{N} [F(a_i)]^{x_i} [1 - F(a_i)]^{1-x_i} \tag{3}$$

where a_i is the damage level (overtopping water depth in this study); x_i=1 or 0 indicates embankment breach or no breach, respectively, under the corresponding damage level; and N is the total number of case histories.

3.2 Railway damage record

3.2.1 Asa River flood of 2010

Locations of ballast and embankment fill scour are determined by investigating photos taken from the factory beside the railway (personal communication with the factory and downloaded from the internet) as well as aerial photos of the area obtained in February 2012.

3.2.2 Sayo River flood of 2009

Kaneko (2010) reported damage to the railway as a function of kilometer post along the track. Site survey data (personal communication with I. Ario), photos from the internet, and aerial photos from October 2009 (immediately after the flood) were also utilized to detail damage along the length of the section of railway.

3.3 Estimation of overtopping water stage

3.3.1 Hydraulic model for flood flow simulation (Tsubaki et al. 2012b)

The river and floodplain flows were calculated by solving the shallow water equations. The basic equations solved here are as follows:

$$\frac{\partial U}{\partial t} + \frac{\partial E}{\partial x} + \frac{\partial F}{\partial y} = S \tag{4}$$

Nat. Hazards Earth Syst. Sci. Discuss., doi:10.5194/nhess-2016-167, 2016
Manuscript under review for journal Nat. Hazards Earth Syst. Sci.
Published: 31 May 2016

$$U = \begin{pmatrix} h & hu & hv \end{pmatrix}^T,$$
$$E = \begin{pmatrix} hu & hu^2 + 0.5gh^2 & huv \end{pmatrix}^T,$$
$$F = \begin{pmatrix} hv & huv & hv^2 + 0.5gh^2 \end{pmatrix}^T,$$
$$S = \begin{pmatrix} q_s & gh(S_{0x} - S_{fx} - S_{Hx}) & gh(S_{0y} - S_{fy} - S_{Hy}) \end{pmatrix}^T. \quad (5)$$

where t is the time, x and y are the horizontal coordinates, h is the water depth, u and v are the depth-averaged velocities in the x- and y- directions, g is the gravitational acceleration, q_s is the source water mass due to rainfall, S_{0x} and S_{0y} are the bed slopes in the x- and y- directions calculated using the ground elevation z as

$$S_{0x} = -\frac{\partial z}{\partial x},\ S_{0y} = -\frac{\partial z}{\partial y}. \quad (6)$$

S_{fx} and S_{fy} are the friction slopes evaluated by using the Manning's roughness coefficient n as follows.

$$S_{fx} = \frac{n^2 u\sqrt{u^2 + v^2}}{h^{4/3}},\ S_{fy} = \frac{n^2 v\sqrt{u^2 + v^2}}{h^{4/3}}. \quad (7)$$

S_{Hx} and S_{Hy} are the energy slope due to the bridge with piers. These terms are effective only at the cell interface located in the bridge cross-section.

$$S_{Hx} = -\frac{\partial H_b}{\partial x},\ S_{Hy} = -\frac{\partial H_b}{\partial y} \quad (8)$$

where H_b is the head loss due to the bridge. The amount of head loss was calculated by using D'Aubuisson's empirical formula (Chow 1959, Sakano 2003, Tsubaki et al. 2012b).

The equations were solved by means of the finite volume method on an unstructured triangular grid. The flux difference scheme (FDS) was used to evaluate fluxes through the boundaries of each triangular cell.

(a) Sayo River model (Tsubaki et al. 2012b)

The domain represented in the inundation simulation (Figure 4, right panel) was about 15 km^2 in area. The Sayo River flows through this section, and no major tributaries are present here. Elevation data for the calculation grid was configured using aerial LiDAR (Light Detection and Ranging) for the riverside region, and a 50-m grid DEM (Digital Elevation Model) was utilized for the intermountain area. A comparatively small grid size (3 m for the length of a side of a triangle) was used around the river and the railway to represent the details of the topography (Bates et al. 2003, Cobby et al. 2003, Rath and Bajat 2004). In the mountain area, a larger grid size (40 m in length) was used to reduce computational load. Manning's roughness parameter n was set to 0.02 for the river bed and the floodplain, 0.1 for vegetated areas of the river course and floodplain as well as for residential areas, and 0.3 for mountainous areas. The discharge estimated by using a hydrological model with the ground rain gauge data (Fujita et al. 2012) was used as the inflow boundary condition. The rating curve at the outflow cross-section was estimated and the flow rate at the outflow cross-section calculated by the hydrological model was converted to water stage. The source term in

Nat. Hazards Earth Syst. Sci. Discuss., doi:10.5194/nhess-2016-167, 2016
Manuscript under review for journal Nat. Hazards Earth Syst. Sci.
Published: 31 May 2016

Natural Hazards and Earth System Sciences
Open Access
Discussions

the mass conservation equation (q_s in Equation (5)) represents the precipitation in this area; the observed gross precipitation is multiplied by a runoff ratio of 0.85 to account for the amount of net surface runoff in this area.

(b) Asa River model

Due to the short length of the river reach (2 km) focused on in this study, and the relatively steep riverbed slope (1/240), the flood was evaluated using a steady peak flow simulation. The inflow rates, based on the flow simulation conducted by Yamaguchi Prefecture, were used as constant inflow boundary conditions for a 2-dimensional unsteady flow model. Resolution of the triangular mesh was 2 m in the area of railway embankment fill, and 5 m elsewhere. Manning's n was set to 0.03 in the river channel and floodplain, and 0.1 in vegetated and built-up areas. This river channel roughness equals that used by Yamaguchi Prefecture in historical analyses. The downstream boundary condition was water level as determined by Yamaguchi Prefecture's calculation (personal communication).

3.3.2 Validation of inundation flow models

To validate the inundation flow models, calculated results are compared with inundation records.

(a) Sayo River model

As shown in Figure 5, the calculated inundation area corresponds closely to the recorded inundation area. In Figure 6, calculated and recorded inundation water stages and water depths are compared. The calculated water stage is represented by $h + z$. The mean absolute error is 0.28 m, and the magnitude of the error is smaller than, but comparable to, the magnitude of inundation water depth, 1 m.

Nat. Hazards Earth Syst. Sci. Discuss., doi:10.5194/nhess-2016-167, 2016
Manuscript under review for journal Nat. Hazards Earth Syst. Sci.
Published: 31 May 2016

Natural Hazards and Earth System Sciences
Open Access
Discussions

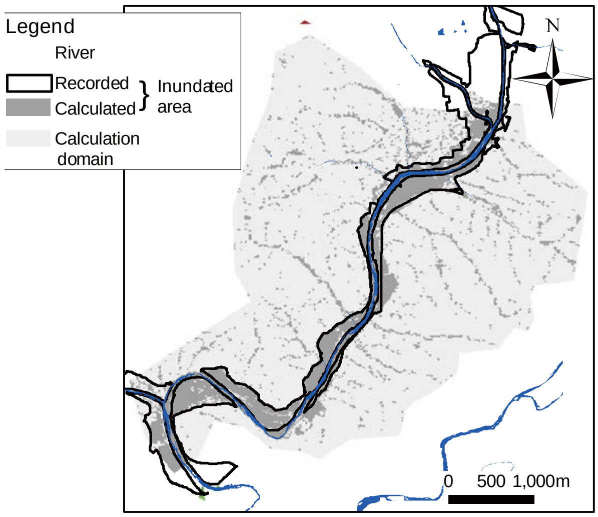

Figure 5 Comparison of calculated and recorded inundated areas (Tsubaki et al. 2012b).

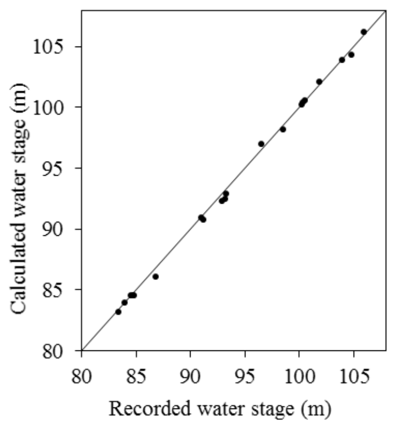

Figure 6 Comparison of calculated and recorded flood stages and depths (Tsubaki et al. 2012b).

(b) Asa River model

Water levels hindcast by the flood simulation are compared with measured water level traces from two locations (Figure 3). Steady flow boundary conditions were used for model inflow and outflow, though the presence of vortices over the floodplain and near the riverbanks prevented perfectly steady flow from forming. Due to these fluctuations, modeled water levels were assessed via both 20-minute running averages representing each minute of model output, as well as maximum water levels during these same intervals. Flood elevation trace #1, on the inner wall of the factory, was measured to be 25.98 m. The average modeled flood elevation here was 25.79 m, and the maximum modeled flood elevation at this location was 25.90 m. At location #2, the recorded trace elevation was 25.81 m, model average elevation was 25.61 m, and model maximum elevation was 25.67 m. Modeled average elevation is about 19 cm too low, and maximum elevation is about 11 cm too low, compared to measured trace elevations.

(c) Uncertainty in flood water stage

According to the benchmarking of a two-dimensional high-resolution (~2 m grid spacing, LiDAR topography based) urban flood model reported by Hunter et al. (2008), the uncertainty in predicted water level among six hydraulic models was assessed as 0.05 m. This is same order of RMSE error in the terrain data they used.

The difference between calculated and recorded water stages in our simulation was 0.1~0.3 m, and this is larger than the water level uncertainty estimated by numerical models reported by Hunter et al. (2008). This discrepancy may be related to larger inaccuracy in the LiDAR data we used due to very uneven terrain and quite complex surface cover, including rails on the railway embankment and vegetation cover on the embankment slope. Moreover, there is a difference in the definitions of calculated and recorded water depths, namely the calculated water depth is a cell averaged quantity but the recorded water depth denotes the local water depth around obstacles; this caused an underestimation of the calculated water depth as shown on the right side of Figure 6.

In summary, the magnitude of uncertainty in flood water stage in this study was non-negligible but inevitable in practice because of the complexity of the topography and uncertainty in the topographic data available. The fragility curve concept can account for the uncertainty in the explanatory variable, surcharge water depth in this study. The effect of uncertainty in water level prediction on the fragility curve will be discussed later.

4. Results

The difference between H and the elevation z of the railroad track is surcharge Δh, which is correlated with the recorded state of damages categorized into “no damage”, ballast scour and embankment scour (Appendix), and fragility curves were developed based on this correlation. Both upstream water depth H and rail track elevation z are derived from the cell-averaged quantities used in the model described in section 3.3.

The elevation of water overtopping the tracks was taken as water surface elevation H averaged over a 2 m diameter area at a distance of 5 m from the center line of the tracks. For the generation of fragility curves "no damage" was defined as cases where the model result showed the tracks were indeed overtopped

Nat. Hazards Earth Syst. Sci. Discuss., doi:10.5194/nhess-2016-167, 2016
Manuscript under review for journal Nat. Hazards Earth Syst. Sci.
Published: 31 May 2016

Natural Hazards and Earth System Sciences
Discussions
Open Access

but where no damage was observed in reality. Accordingly, the point where neither overtopping was observed nor track damage was recorded was excluded. As such, 10 data points were obtained for the Asa River, and 24 data points for the Sayo River.

Figure 7 displays the fragility curves for the embankment fill scour using the normal distribution (depicted by the dashed line and the log-likelihood = -7.3) and the log-normal distribution (the solid line and log-likelihood = -7.9) resulting from data points at which either no damage (the number of sample was *n*=8) or embankment fill scour (*n*=16) were observed. In Figure 7, open symbols represent individual data points, while filled figures represent overtopping surcharge and damage data which have been put through a 5-point running average after ordering by surcharge. Though both normal and log-normal distribution models (solid and dashed lines, respectively) represent well the trend of damage probability based on the field record (filled circles), the normal distribution has a slightly better fit.

Figure 8 shows a normal fragility curve for ballast scour (dashed line, log-likelihood = -2.6) and a log-normal curve for the combination of ballast and embankment scour (thick line, log-likelihood = -8.9). For the case of ballast scour, the fits of the normal distribution and the log-normal distribution were almost identical. As shown in Figure 8, the fragility curve for ballast scour has a larger mean and smaller standard deviation compared with the curve for embankment scour and the curve for combined ballast and embankment scour. The failure probability at medium surcharge depth 0.2 m<Δh<0.6 m for the combined ballast and embankment scour is slightly larger than the probability for embankment scour only.

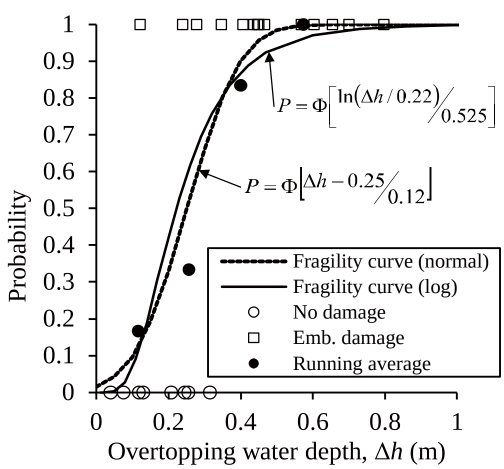

Figure 7 Fragility curves for embankment scour damage described by normal and log-normal distributions.

Nat. Hazards Earth Syst. Sci. Discuss., doi:10.5194/nhess-2016-167, 2016
Manuscript under review for journal Nat. Hazards Earth Syst. Sci.
Published: 31 May 2016

Natural Hazards and Earth System Sciences
Open Access
Discussions

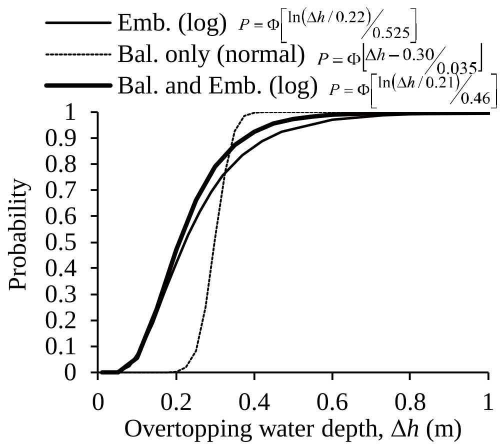

Figure 8 Fragility curves for ballast scour (Bal. only), embankment scour (Emb.) and ballast and embankment scour (Bal. and Emb.)

5. Discussion

5.1 Consistency in lower limit of failure probability with experimental result

Ballast damage is a transitional type of damage, falling between "no damage" and embankment fill scour in its severity. The number of samples with ballast damage available in this study is limited (*n*=7) because this type of damage occurred in between sections with embankment fill scour and "no damage". During a full-scale experiment of ballast scour (Tsubaki et al. 2012a), steady scour was observed beginning at a flow rate per unit length of q_c=0.045 m^2/s. Figures 7 and 8 show surcharge depth on the x-axis, but there is a relation between surcharge depth and overtopping flow rate. By adopting the broad-crested weir concept, the overtopping discharge per unit length can be estimated as

$$q = \alpha \Delta h^{3/2} \qquad (9)$$

where α= 2.46 to 3.47 and Δh is the surcharge water depth above the weir crest (Chow, 1959). Using equation (9) and α= 2.46, the overtopping water depth is converted to the overtopping flow rate per unit length in Figure 9. In this figure, the critical flow rate for ballast scour is depicted as a vertical dashed line. This critical flow rate corresponds well to the initial rise of the log-normal fragility curve for embankment and ballast scour. The agreement of the initial rise of the fragility curve of embankment/ballast scour and critical flow rate to initiate ballast scour indicates that railway overtopping damage begins with ballast scour and progresses to embankment scour. This also implies that the critical flow rate for initiation of ballast scour based on the full-scale experiment of ballast scouring conducted by Tsubaki et al. (2012a) can be used as a critical condition for initiation of railway

Nat. Hazards Earth Syst. Sci. Discuss., doi:10.5194/nhess-2016-167, 2016
Manuscript under review for journal Nat. Hazards Earth Syst. Sci.
Published: 31 May 2016

ballast damage in the field.

5.2 Upper limit of failure probabilities

The upper limit of the overtopping flowrate at which no-damage was observed in the assessment in previous sections is depicted as a double line in Figure 9. The damage probability is almost identical for both models at this upper limit. Above this flow rate, the probability of combined ballast and embankment scour increases slowly due to the assumed shape of the distribution and uncertainty at lower flow conditions (q < 0.2 m^2/s and Δh < 0.2 m). Actually, an overtopping flow rate of 0.5 m^2/s (corresponding to a surcharge of 0.4 m) is quite an intense flow from the viewpoint of earthen embankment overtopping, and it is very unlikely that no scour will be occur during such an intense flow.

5.3 On the deviation of probabilities

In Figure 8, the fragility curve for ballast scour has a median surcharge of Δh=0.29 m, and its variance σ = 0.035 m is smaller than those for the embankment scour model and the fragility curve for combined damage. It must be kept in mind that the LiDAR topography used in the flood model has a RMSE on the order of 0.1 m, and the uncertainty in hindcast flood levels was on the order of 0.2 m, so the standard deviation σ = 0.035 m of the ballast scour model is very small compared with expected uncertainty in the estimated surcharge level. The experiment of Tsubaki et al. (2012a) showed ballast scour to begin at q_c = 0.045 m^2/s, which is an order of magnitude smaller than the median (q = 0.4 m^2/s) or lower limit (q = 0.25 m^2/s) of the fragility curve for ballast scour shown in Figure 9. Therefore, it appears the calculated fragility curve for ballast breach in this study may overestimate the condition experimentally evaluated in Tsubaki et al. (2012). This may partially be explained by the fact that the ballast embankment in the field had been consolidated due to periodical loading by railcars, and because actual ballast may have greater resiliency than in the experiment conducted by Tsubaki et al. (2012a). Even so, ballast should be more vulnerable to overtopping scour than embankment fill is, but the fragility curves shown in Figure 9 did not correspond to such a relation. It is also possible that, in the field cases studied, ballast scour at smaller overtopping flowrates always coincided with combined ballast and embankment scour, not ballast scour alone. Future work is needed to improve the fragility curve for ballast scour by acquiring more sample data points in the field and running more hydraulic experiments.

Nat. Hazards Earth Syst. Sci. Discuss., doi:10.5194/nhess-2016-167, 2016
Manuscript under review for journal Nat. Hazards Earth Syst. Sci.
Published: 31 May 2016

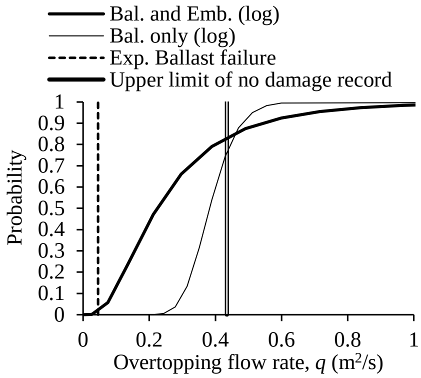

Figure 9. Fragility curve for ballast failure using overtopping flow rate per unit length. The dashed line indicates the experimental bound at which the onset of ballast scour occurs (Tsubaki et al. 2012a). The double line corresponds to the upper limit of the flow condition where no-damage was observed.

5.4 Validation of railway fragility curve

A validation of the combined damage fragility curve, of which feasibility was discussed in sections 5.1 to 5.3, was conducted by comparing its calculated probabilities to the actual damage record. The log-normal distribution for ballast and embankment scour was determined to be the most feasible model. Via the model, the failure probability along the rail-track in the Asa River floodplain at 10 m intervals was calculated and plotted in Figure 10 (left). Failure probability in Figure 10 (left) is calculated without regard to type of failure (embankment fill or ballast), but is calculated with the lumped damage curve; however, the actual damage record of the right figure distinguishes the type of damage. In Figure 10, there is variability in the calculated result, but it generally agrees with recorded damage. The points at which no damage was calculated are points at which the flood model calculated either a very shallow overtopping surcharge, or no overtopping at all. The railway crest in this section is almost horizontal, with little large-scale topographic variation. Since the crest of the railway embankment consists of both rail and railway ties (sleepers), the 1 m^2 resolution LiDAR data cannot resolve this, and the 1.7 m^2 triangular mesh carries forward this variation, leading to an unavoidable difference between modeled and actual topography. Since actual railroad crest elevation does not experience spurious variations at 10 m intervals, topography based on LiDAR data of limited resolution and accuracy might be improved by application of a spatial filter along the railway.

Nat. Hazards Earth Syst. Sci. Discuss., doi:10.5194/nhess-2016-167, 2016
Manuscript under review for journal Nat. Hazards Earth Syst. Sci.
Published: 31 May 2016

Natural Hazards and Earth System Sciences
Open Access
Discussions

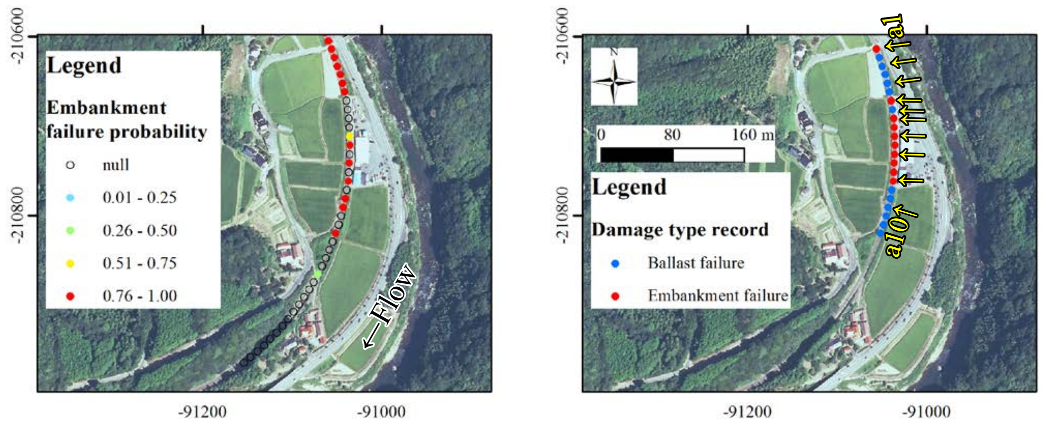

Figure 10 Estimated damage probability (left) and damage record (right) at Asa River section M. The yellow symbols in the right map depict data points listed in Table A.1.

Figure 11 shows calculated and observed damage to the railway along the Sayo River. The domain is decomposed into two segments (A and B) in the discussion below. Continuous damage was recorded along a portion of Segment A, and this damage was reproduced well in the fragility curve calculation. In this segment, damage occurred in locations at which relatively steep slopes existed in the railway crest elevation profile (Figure 12). Since the locations of railway embankment overtopping were governed by longitudinal slope of the railway and large-scale topography in this segment A, the flood model was able to simulate actual overtopping location and flow rate with good accuracy, and damage probability resulting from the fragility curve matched recorded damage well. In Segment B, estimated damage probability was high at points that experienced actual damage, but many other points with high damage probability experienced no actual damage. In regions such as this, where spatially sporadic damage is calculated, fragility curves are still useful for predicting whether damage will occur, but they cannot predict the specific locations at which the damage should be expected. In this segment, elevation of the railway embankment crest was very smooth, with no steep slopes in crest elevation. Therefore, the entire segment was overtopped with shallow surcharge. However, small errors in topography at the size of each model grid cell caused errors in the overtopping surcharge depth, resulting in different damage probabilities at the 10 m intervals at which damage was assessed. The fragility curve concept can also account for uncertainty in hazard level; in segments within which sporadic damage is predicted, the level of damage can be estimated by averaging the damage predicted for points within the segment. However, the reason damage in Segment B of Figure 11 was not evaluated as such an average is that the error in grid-scale model topography was too large to just cause variations in overtopping surcharge depth; rather, the error caused many points within the segment to not experience any overtopping at all. Therefore,

Natural Hazards and Earth System Sciences
Open Access
Discussions

the model predicted scattered damage for Segment B.

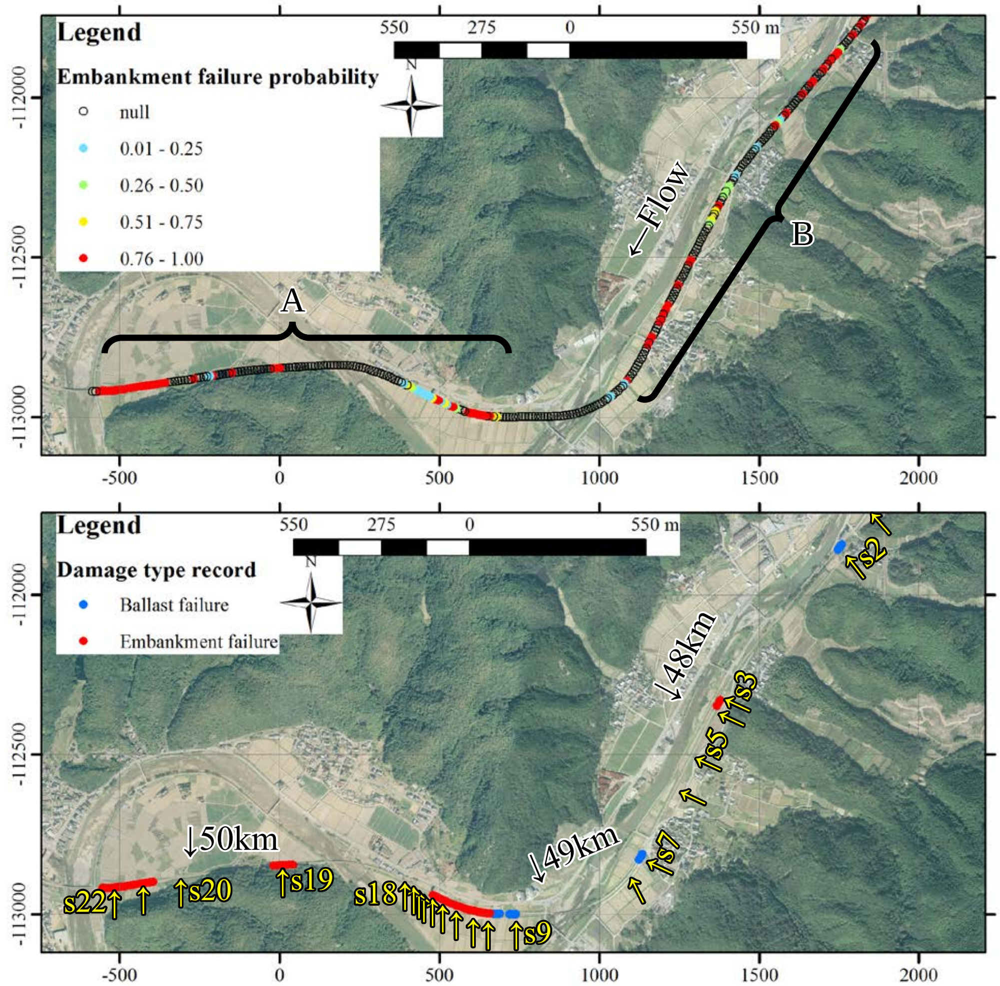

Figure 11 Estimated damage probability (top) and damage record (bottom) at Sayo River section S. The yellow symbols in the bottom figure depict data points listed in Table A.2.

Nat. Hazards Earth Syst. Sci. Discuss., doi:10.5194/nhess-2016-167, 2016
Manuscript under review for journal Nat. Hazards Earth Syst. Sci.
Published: 31 May 2016

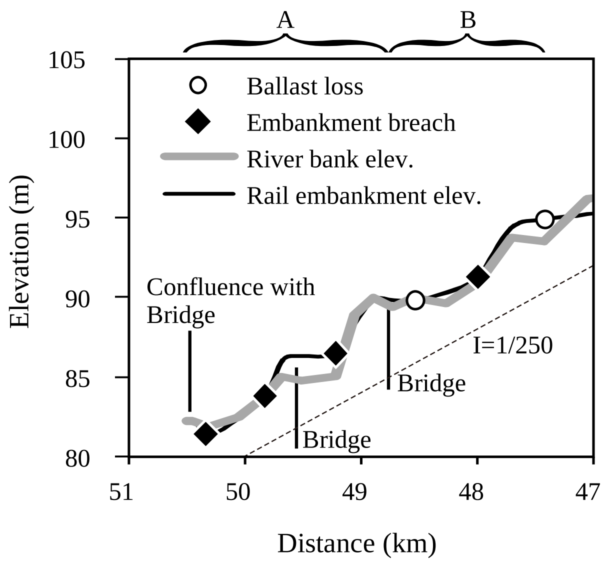

Figure 12 Longitudinal profiles of railway and riverbank elevation. The cross-sections where the river and railway intersect are indicated as 'bridge' (Tsubaki et al. 2012b).

6. Conclusion

This paper shows the significance of evaluating the likelihood of damage to railway embankments due to overtopping. Fragility curves were developed to relate damage probability to overtopping surcharge depth, itself calculated via the use of a hydraulic flood model. Fragility curves were generated based on recorded observations of railway damage types, simulated overtopping surcharge and types of curve. Each fragility curve was validated by comparison between modeled damage probability and records of observed damage. The fragility curve for ballast scour, the least serious type of damage investigated, did not match the criteria revealed through laboratory experiments of ballast scour, and may underestimate actual damage probability. However, the fragility curve for combined damage including embankment fill and ballast scour well represents the laboratory experiment result for the onset of scour. Field validation of the combined damage fragility curve was carried out by comparing modeled damage probability with recorded damage at two different river sections. At one location, where recorded damage indicated continuous railway washout over stretches, fragility curve damage probability agreed with observed damage quite well. On the other hand, the model did not well represent observed damage in locations of relatively flat and level railway crest, where variations in the simulated overtopping surcharge depth were affected by small errors in the topographic data, resulting in sporadic flood overtopping where no damage existed in reality.

Though the fragility curves developed here are useful for estimation of damage probability for single-track non-electrified railroad embankments, the limited number of data points used to generate these curves prevents them from being applicable to a variety of situations. To make these curves more robust, more field records are needed in different types of environments. Furthermore, the fit of modeled ballast scour probability to observed ballast damage was unsatisfactory, indicating the necessity for further laboratory experiments and field data collection. In addition, the role of small errors in the hydraulic flood model result on predicted damage probability has become clear, and the application of spatial filtering to improve model accuracy needs to be investigated in the future.

Appendix

Table A.1 Pointwise estimated overtopping water depth Δh and damage record for the Asa River flood. (In status row, emb: embankment breaching, bal: ballast breaching and no: no damage, accordingly.)

point	calc z(m)	calc H(m)	Δh(m)	status
a1	26.89	27.36	0.47	emb
a2	26.94	27.35	0.41	bal
a3	26.94	27.35	0.41	bal
a4	26.90	27.35	0.45	emb
a5	26.99	27.34	0.35	bal
a6	27.00	27.35	0.35	emb
a7	26.94	27.35	0.41	emb
a8	26.90	27.35	0.45	emb
a9	26.91	27.35	0.44	emb
a10	26.93	27.34	0.41	bal

Table A.2 Pointwise estimated overtopping water depth Δh and damage record for the Sayo River flood.

point	calc z(m)	calc H(m)	Δh(m)	status
s1	95.56	95.88	0.31	no
s2	94.96	95.30	0.34	bal
s3	91.55	91.83	0.28	emb
s4	91.12	91.36	0.24	emb
s5	90.85	90.98	0.13	no
s6	90.50	90.98	0.48	no
s7	89.88	90.37	0.49	bal
s8	89.85	90.10	0.25	no
s9	87.65	87.93	0.28	bal
s10	87.37	87.94	0.57	emb
s11	85.82	87.27	1.46	emb
s12	86.04	87.35	1.31	emb
s13	86.52	87.31	0.80	emb
s14	86.36	86.48	0.12	emb
s15	86.17	86.21	0.04	no
s16	86.24	86.31	0.08	no
s17	86.16	86.27	0.12	no
s18	82.34	82.55	0.21	no
s19	81.87	82.57	0.70	emb
s20	82.31	82.55	0.25	no
s21	81.91	82.57	0.66	emb
s22	81.96	82.56	0.60	emb

Acknowledgement

The authors thank Martin Judd at New Jersey Transit for providing us information about railway system damage due to storm surge. Our study was partially funded by the JSPS-NSF Cooperative Program for Interdisciplinary Joint Research Projects in Hazards and Disasters, project entitled "Evolution of Urban Regions in Response to Recurring Disasters", a grant from the Chugoku Civil Engineering Foundation for Mutual Aid, Japan, and a grant from the Foundation for River and Watershed Environment Management, Japan.

References

Argyroudis, S. and Kaynia, A.M., 2014. Fragility functions of highway and railway infrastructure. In SYNER-G: typology definition and fragility functions for physical elements at seismic risk (pp. 299-326). Springer Netherlands.

Bates, P.D., Marks, K.J., Horritt, M.S., 2003. Optimal use of high-resolution topographic data in flood inundation models, Hydrological processes, Vol.17, pp.537-557.

Brammer, H., 1990. Floods in Bangladesh: II. Flood mitigation and environmental aspects. Geographical Journal, pp.158-165.

Changnon, S.A., 2009. Impacts of the 2008 floods on railroads in Illinois and adjacent states. Transactions of the Illinois State Academy of Science, 102(3-4), pp.181-191.

Chow, V.T., 1959. Open-channel hydraulics, McGraw Hill Book Company (reprinted by Blackburn Press).

Cobby, D.M. et al. Mason, D.C., Horritt, M.S., Bates, P.D., 2003. Two-dimensional hydraulic flood modeling using a finite-element mesh decomposed according to vegetation and topographic features derived from airborne scanning laser altimetry, Hydrological processes, Vol.17, pp.1979-2000.

Federal Emergency Management Agency, 2010a. Earthquake model, Hazus®-MH MR5 technical manual.

Federal Emergency Management Agency, 2010b. Flood model, Hazus®-MH MR5 technical manual.

Federal Emergency Management Agency, 2010c. Hurricane model, Hazus®-MH MR5 technical manual.

Fujita, I., Ito, T. and Sayama, T., 2012, Inundation Analysis of 2009 Chikusa River Flood and Comparison of Evacuation Criteria, Journal of Flood Risk Management, DOI: 10.1111/jfr3.12020.

Hall, J.W., Dawson, R.J., Sayers, P.B., Rosu, C., Chatterton, J.B. and Deakin, R., 2003, September. A methodology for national-scale flood risk assessment. In Proceedings of the Institution of Civil Engineers-Water Maritime and Engineering (Vol. 156, No. 3, pp. 235-248). London: Published for the

Nat. Hazards Earth Syst. Sci. Discuss., doi:10.5194/nhess-2016-167, 2016
Manuscript under review for journal Nat. Hazards Earth Syst. Sci.
Published: 31 May 2016

Institution of Civil Engineers by Thomas Telford Ltd., c2000-c2003.

Hata, Y., Sakai, H., Shizuma, T., Nozu, A., Ichii, K. and Maruyama, Y., 2015. Evaluation of Fragility Curve on Traffic Function of River Dike Based on Strong Motion Estimation Considering Empirical Site Amplification and Phase Effects -The Case of the Naruse River Dike for the Past Large Scale Earthquakes -. Journal of Japan Society of Civil Engineers, Ser. A1 (Structural Engineering & Earthquake Engineering (SE/EE)), 71, pp.894-914 (in Japanese).

Hunter, N.M., Bates, P.D., Neelz, S., Pender, G., Villanueva, I., Wright, N.G., Liang, D., Falconer, R.A., Lin, B., Waller, S. and Crossley, A.J., 2008. Benchmarking 2D hydraulic models for urban flood simulations. In Proceedings of the Institution of Civil Engineers: Water Management (Vol. 161, No. 1, pp. 13-30). Thomas Telford (ICE publishing).

Ichii, K., 2002. A seismic risk assessment procedure for gravity type quay walls. Structural Engineering/Earthquake Engineering, 19(2), pp.131S-140S.

Intergovernmental Panel on Climate Change, 2014. Climate Change 2014: Synthesis Report. Contribution of Working Groups I, II and III to the Fifth Assessment Report of IPCC, edited by Pachauri, R.K. et al.

Kaneko, Y., 2010. The damages to the railway of the Kishin line between Kyutoku station to Mimasakadoi station due to the typhoon Etau, J. of Japan Rail Way Civil Eng. Association, 6, 450-451. (in Japanese)

Onoda, H. and Hayano, K., 2015. SPH simulation of railroad ballast bed slope collapse under inundation flow. Journal of Japan Society of Civil Engineers, Ser. E1 (Pavement Engineering), 71(2). (in Japanese)

Polemio, M. and Lollino, P., 2011, Failure of infrastructure embankments induced by flooding and seepage: a neglected source of hazard, Natural Hazards and Earth System Sciences, 11, 3383-3396.

Rath, S., Bajat, B., 2004. Between sensing, Forecasting and risk assessment: an integrated method to model high resolution data for floodplain representations in hydrodynamic simulations, Proceedings of the 1st Goettingen Remote Sensing Days, Goettingen.

Reed, D.W., Webb, B., Arnell, N., Onof, C., MacIntyre, N., Gurney, R. and Kirby, C., 2004. A review of British railway bridge flood failures. In Hydrology: science and practice for the 21st century. Proceedings of the British Hydrological Society International Conference, Imperial College, London, July 2004. (pp. 210-216). British Hydrological Society.

Sakano, A., 2003. Hydraulic study on accumulation of drifting wood at a bridge during a flood, Technical note of National Institute for Land and Infrastructure Management, No.78. (in Japanese)

Shimozono, T., and Sato, S., 2016. Coastal vulnerability analysis during tsunami-induced levee overflow and breaching by a high-resolution flood model. Coastal Engineering, 107, 116-126.

Shinozuka, M., Feng, M.Q., Lee, J. and Naganuma, T., 2000. Statistical analysis of fragility curves. Journal of Engineering Mechanics, 126(12), pp.1224-1231.

Suppasri, A., Mas, E., Koshimura, S., Imai, K., Harada, K. and Imamura, F., 2012. Developing tsunami fragility curves from the surveyed data of the 2011 Great East Japan tsunami in Sendai and Ishinomaki plains. Coastal Engineering Journal, 54(01), p.1250008.

Tsubaki, R., Kawahara, Y. and Ueda, Y., 2012a. An experimental study on railway embankment breach and its critical flow condition, 18th Congress of the Asia and Pacific Division of the IAHR, On USB memory, Jeju, Korea, August.

Tsubaki, R., Kawahara, Y., Sayama, T. and Fujita, I., 2012b, Analysis of geomorphic and hydraulic conditions causing railway embankment breach due to inundation caused by heavy rainfall, Journal of Hydraulic and Hydroscience Engineering, JSCE, 30(1), 87-99,.

Tsubaki, R. and Kawahara, Y., 2013. The uncertainty of local flow parameters during inundation flow over complex topographies with elevation errors, Journal of Hydrology, Vol. 486, 10.1016/j.jhydrol.2013.01.042.

Tsubaki, R., Asai, K., Nakamura, A., Tomura, K., Kawahara, Y. and Nagano, H., 2014. Inundation Flow in Mountainous Village in ASA River Basin during 2010 July Torrential Rainfall Event, Journal of Japan Society of Civil Engineers, Ser. B1 (Hydraulic Engineering), 70, p.1441.

Ueda, N. and Nakatsuka, H., 2014. The circumstances and the effect of synthetic submersion-under-water damage mitigation measures (Second Dike etc.) in Hijikawa (East Ozu Area), River (Kasen), 70(10), pp.24-27. (in Japanese)

Vorogushyn, S., Merz, B. and Apel, H., 2009. Development of dike fragility curves for piping and micro-instability breach mechanisms. Natural Hazards and Earth System Sciences, 9(4), pp.1383-1401.

Wardhana, K. and Hadipriono, F.C., 2003. Analysis of recent bridge failures in the United States. Journal of Performance of Constructed Facilities, 17(3), pp.144-150.